Exploration of magnetic perturbation effects on advanced divertor configurations in NSTX-U

H. Frerichs, O. Schmitz, I. Waters, G. P. Canal, T. E. Evans, Y. Feng, and V. A. Soukhanovskii

Citation: Physics of Plasmas **23**, 062517 (2016); doi: 10.1063/1.4954816
View online: http://dx.doi.org/10.1063/1.4954816
View Table of Contents: http://scitation.aip.org/content/aip/journal/pop/23/6?ver=pdfcov
Published by the AIP Publishing

Exploration of magnetic perturbation effects on advanced divertor configurations in NSTX-U

H. Frerichs,[1] O. Schmitz,[1] I. Waters,[1] G. P. Canal,[2] T. E. Evans,[2] Y. Feng,[3] and V. A. Soukhanovskii[4]
[1]*Department of Engineering Physics, University of Wisconsin-Madison, Madison, Wisconsin 53706, USA*
[2]*General Atomics, San Diego, California 92186, USA*
[3]*Max-Planck Institute for Plasma Physics, Greifswald, Germany*
[4]*Lawrence Livermore National Laboratory, Livermore, California 94551, USA*

(Received 18 April 2016; accepted 10 June 2016; published online 29 June 2016)

The control of divertor heat loads—both steady state and transient—remains a key challenge for the successful operation of ITER and FNSF. Magnetic perturbations provide a promising technique to control ELMs (Edge Localized Modes) (transients), but understanding their detailed impact is difficult due to their symmetry breaking nature. One approach for reducing steady state heat loads is so called "advanced divertors" which aim at optimizing the magnetic field configuration: the snowflake and the (super-)X-divertor. It is likely that both concepts—magnetic perturbations and advanced divertors—will have to work together, and we explore their interaction based on the NSTX-U setup. An overview of different divertor configurations under the impact of magnetic perturbations is presented, and the resulting impact on plasma edge transport is investigated with the EMC3-EIRENE code. Variations in size of the magnetic footprint of the perturbed separatrix are found, which are related to the level of flux expansion on the divertor target. Non-axisymmetric peaking of the heat flux related to the perturbed separatrix is found at the outer strike point, but only in locations where flux expansion is not too large. *Published by AIP Publishing.* [http://dx.doi.org/10.1063/1.4954816]

I. INTRODUCTION

The control of divertor heat loads—both steady state and transient—remains a key challenge to design a viable fusion power plant. Both suppression and mitigation of transient heat loads (so called ELMs, Edge Localized Modes) by application of non-axisymmetric magnetic perturbations from dedicated external control coils have been observed in several tokamaks,[1–3] which make this method an essential part of ELM control in the next step fusion device ITER.[4,5] Furthermore, magnetic perturbations can be used to trigger ELMs on demand.[6] The detailed exploration of both resonant magnetic perturbation (RMP) and non-resonant magnetic perturbation effects, however, is still an ongoing process, and it is complicated by their symmetry breaking nature: the magnetic separatrix splits into two distinct branches (invariant manifolds) which begin to oscillate when approaching the X-point in either forward or backward direction[7,8] (see sketch in Figure 1). These branches provide an envelope for magnetic field lines than connect from the plasma interior to the divertor targets, and they intersect the divertor targets in a non-axisymmetric pattern. As a result, splitting of the steady state heat and particle flux strike points can be observed.[9,10] While most of the tokamak edge transport codes such as SOLPS and UEDGE are based on an axisymmetric idealization of the configuration (e.g., neglecting toroidal field ripple effects) allowing for a two-dimensional model, a full three-dimensional model is required to analyze ELM control experiments in detail. The full three-dimensional setup is taken into account by the EMC3-EIRENE code,[11,12] which is used for related plasma edge transport studies in non-axisymmetric configurations at DIII-D,[13] ASDEX-Upgrade,[14] NSTX,[15] and ITER.[16]

While resonant magnetic perturbations (RMPs) were originally considered for the control of steady state particle and energy exhausts by "ergodization" of the boundary layer[17,18] (i.e., ergodic limiter), they act only as a supplement to poloidal divertors for fine tuning edge transport in the present fusion devices. Presently, another approach for a reduction of steady state heat loads is pursued: so called "advanced divertors" which aim at optimizing the equilibrium (axisymmetric) magnetic field configuration. One such configuration is the "snowflake" divertor[19] in which the poloidal magnetic field null approaches second order, resulting in a characteristic hexagonal form of the separatrix and thus introducing two additional strike points intended for heat load spreading. Another configuration is the X-divertor,[20] which aims at flaring the field lines near the divertor plates and thus reducing heat loads. By increasing the major radius of the strike point, the super-X divertor[21] is considered to reduce heat loads even further.

It is likely that both concepts—magnetic perturbations and advanced divertors—will have to work together. Such configurations can be investigated in NSTX-Upgrade (NSTX-U): magnetic perturbations can be generated by a set of 6 midplane coils, and access to advanced divertor configurations is provided by additional poloidal field coils. We will begin with an overview of different advanced divertor configurations at NSTX-U in Section II since we will see that the oscillations of the perturbed separatrix manifolds depend on certain properties of the equilibrium configuration. The interaction of magnetic perturbations with these advanced divertor configurations is then analyzed in Section III: the separatrix manifolds and their footprints on the divertor plates are introduced. The resulting

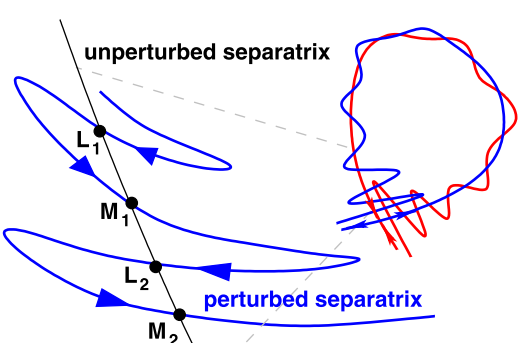

FIG. 1. Sketch of the perturbed separatrix manifolds (red and blue), and close-up of the lobe structure from oscillations around the unperturbed separatrix. Outward and inward crossing points are marked *L* and *M*, respectively.

impact on the edge plasma with a focus on divertor heat loads is explored with the EMC3-EIRENE code in Section IV.

II. ADVANCED DIVERTOR CONFIGURATIONS

We begin with a general discussion on the classification scheme of advanced divertors and then look at implementations at NSTX-U in more detail.

A. Classifications

The so called "snowflake" (SF) divertor, with its characteristic hexagonal shape of the separatrix, introduces two additional strike points which may facilitate heat flux spreading. Furthermore, it provides a larger divertor volume due to flux expansion near the magnetic null, and it facilitates longer field line connection lengths. However, it has been recognized early on that the exact configuration with its second order magnetic null is topologically unstable with respect to small fluctuations in the plasma or divertor currents. Operating at lower or higher divertor currents leads to configurations with two first order magnetic nulls:[22] the "snowflake-minus" (SF-) configuration has two neighboring X-points on the separatrix (see Figure 2(a)), and the "snowflake-plus" (SF+) configuration has a secondary X-point below the primary one in the private flux region (see Figure 2(b)). Further generalization of the relative position of the two first order nulls has been introduced in Ref. 23 (e.g., Figure 5), resulting in the following classifications:

(1) The (original) "symmetric snowflake-minus" with two X-points on the separatrix facing the core plasma,
(2) The "asymmetric snowflake-minus" (aSF-) configuration with a secondary X-point somewhere in the scrape-off layer (SOL) (see Figure 2(f)),
(3) The "tilted symmetric snowflake-minus" (tsSF-) configuration with a second X-point on one of the separatrix legs below the primary X-point (i.e., not in contact with the core plasma, see Figure 2(e) approximately), and
(4) The "snowflake-plus" (SF+) configurations with a secondary X-point in the private flux region (it can be further divided into a symmetric configuration in which the second X-point is strictly below the primary one on its

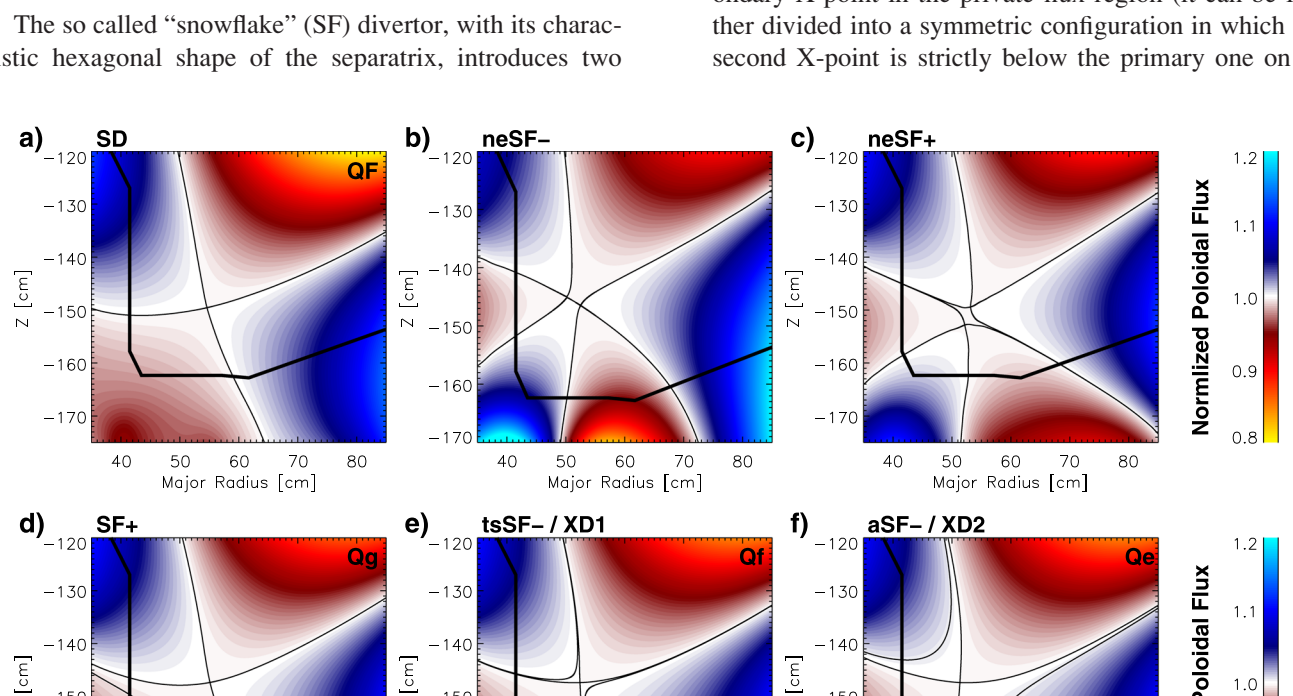

FIG. 2. The standard divertor (SD) reference configuration (a) and an overview of different near exact and generalized "snowflake" configurations in NSTX-U: (b) and (c) near exact SF (neSF) configurations approximated as SF- and SF+, respectively, (d) a "snowflake plus" (SF+) configuration, (e) a "tilted symmetric snowflake minus" (tsSF-) configuration, and (f) an "asymmetric snowflake minus" (aSF-) configuration. These equilibrium configurations are taken from the 116313/NfHz0+Q series, except for neSF-which is 135111/Nwj_08.

symmetry axis, and the asymmetric configuration in which the second X-point is to either side of the symmetry axis, but this does not affect the magnetic topology).

(5) The "classical snowflake" configuration is the limit when both first order magnetic nulls are brought together and merge to one second order magnetic null.

These classifications are based exclusively on the magnetic topology without taking into account the position of the divertor plates. Considering different locations for divertor plates will increase the number of configurations even further, and such an enhanced classification scheme is probably necessary to address the resulting differences in divertor operation properties.

The X-divertor, on the other hand, was introduced with the specific intention to flare magnetic field lines downstream from the plasma by introducing an additional X-point near the divertor plate(s).[20] This definition of a divertor configuration explicitly takes into account the relative position of the divertor plates to the secondary X-point. Its focus is on the strike point area, and it can be applied individually for both divertor legs (or all 4 in case of a double null configuration).

Despite a completely different origin of the snowflake and X-divertor concepts (generation of second order magnetic null with increased connection lengths vs. field line flaring near the divertor plates, and by splitting of remote poloidal field coils vs. near target dipole coils), it has been recognized[24] that magnetic configurations exist which share properties of both concepts: an asymmetric or tilted snowflake minus configuration does fulfill the geometric properties of an X-divertor for one divertor leg, if the secondary X-point is located just behind the divertor plates. A discussion of this similarity can be found in recent literature.[25,26]

B. Divertor configurations in NSTX-U

The Upgrade to NSTX provides access to a variety of divertor configurations.[27] A set of NSTX-U equilibria has been modeled in analogy to the snowflake configuration scan in Figure 5 in Ref. 23; an overview is given in Figure 2. These model equilibria are taken from the 116313/NfHz0+Q series which have been generated for a cryo pump study. They are based on a central toroidal field of $B_{\mathrm{tor}} = 1\,\mathrm{T}$ and a plasma current of $I_p = 2\,\mathrm{MA}$, and the shape is characterized by an upper and lower elongation of $\kappa_u \approx 2.4$ and $\kappa_l \approx 2.7$, respectively, and an upper and lower triangularity of $\delta_u \approx 0.39$ and $\delta_l \approx 0.69$, respectively.

Access to the classical snowflake configuration with its second order magnetic null is challenging since it is topologically unstable. A near exact configuration has been generated based on the 116313/NfHz0+Q series (case neSF+ in Figure 2), and another approximation has been modeled previously in a separate study (135111/Njw_08, Figure 2(b)). In the latter approximation features, a second order null which has split into two first order nulls located approximately 2 cm apart on the same separatrix. Topologically, this falls into the "snowflake minus" category, but approximations like this are referred to as "near exact snowflake." The present equilibrium is supported by a central toroidal field of $B_{\mathrm{tor}} = 1\,\mathrm{T}$ and a plasma current of $I_p = 1\,\mathrm{MA}$, its shape is characterized by an elongation of $\kappa_u \approx 2.2$, $\kappa_l \approx 2.6$ and $\delta_u \approx 0.41$, $\delta_l \approx 0.78$.

Before we address RMP application in those configurations, we give a short characterization of the axisymmetric divertor configuration in comparison to the standard divertor (SD) configuration. Characteristic quantities are the poloidal flux expansion factor F and the field line connection length L_c.

1. Poloidal flux expansion

The poloidal flux expansion factor is an indication of how heat (and particle) flux from the midplane is distributed on the divertor targets. It is defined by the ratio of the downstream to upstream distance from the separatrix for a given flux surface, and consequently, it has a radial dependence. Let d_{mid} be the distance from the separatrix at the low field side midplane, and then we can define flux expansion factors on the (outer) target as

$$F_{\mathrm{target}} = \frac{d_{\mathrm{target}}}{d_{\mathrm{mid}}}, \tag{1}$$

where d_{target} is the distance from the outer strike point (OSP) along the divertor target.

While the near exact snowflake configurations do have a large flux expansion right next to the X-point, projecting the flux surface down to the divertor target (Figure 3(a)) shows that F_{target} is smaller than in the standard divertor reference configuration, and this may be of great concern for the distribution of heat loads. The target flux expansion in the neSF+ configuration (magenta) is reduced by a factor of 2, and by a factor of 4–5 in the neSF-configuration (red). These configurations have two secondary strike points

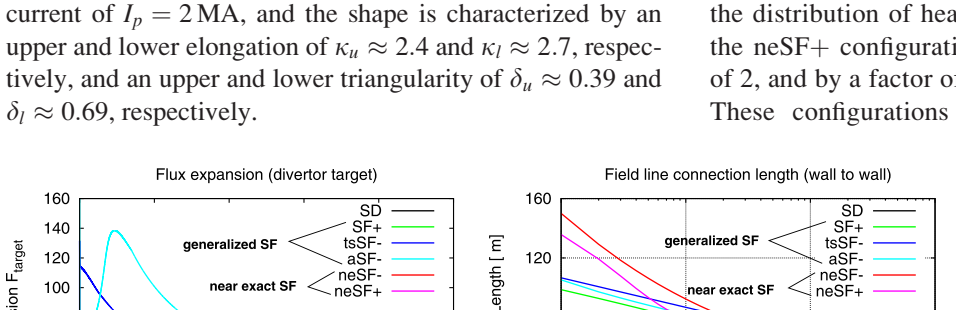

FIG. 3. (a) Flux expansion and (b) field line connection length at the outer divertor target.

which may take over some of the head load. An analysis of heat loads will be presented in Secs. IV A and B.

The picture is significantly different for the "generalized" snowflake configurations (Figures 2(d)–2(f)). These do not have the secondary strike points since the secondary X-point is already behind the wall. This secondary X-point is located in the far private flux region (PFR) in the SF+ configuration (green), which has a slightly improved flux expansion over the SD reference configuration. Thus, "improved standard divertor" is probably a more adequate classification rather than "snowflake plus." The two SF-configurations (blue and cyan), on the other hand, feature a considerably larger flux expansion, which is related to the proximity of the secondary X-point to the outer strike point. This divertor flux expansion is a characteristic feature of X-divertors.

2. Connection length

A qualitative difference in the asymptotic behavior of the field line connection length L_c can be seen in Figure 3(b): the divergence of L_c when approaching the separatrix is much faster in the near exact snowflake configurations than in all other configurations. However, while L_c in the neSF-configuration (red) remains larger than in the SD configuration, it drops below this reference in the neSF+ (magenta) configuration only 3 mm away from the separatrix strike point. This corresponds to less than 0.2 mm upstream, which is probably too small to allow for much dissipation of the power entering the divertor.

The "generalized" snowflake configurations have a moderately larger connection length than the reference configuration throughout most of the divertor target, and only L_c(SF+) approaches the reference L_c(SD) at $d_{\text{target}} \approx 4$ cm.

III. PERTURBED MAGNETIC CONFIGURATIONS

NSTX-U is equipped with a set of 6 midplane coils which can be used to apply non-axisymmetric perturbation fields with toroidal mode number $n = 1 - 3$. Such non-axisymmetric perturbations play an important role in the ELM control design for ITER.[4,28,29] While advanced divertor configurations are traditionally considered axisymmetric (and while the "snowflake" configuration may or may not have its own impact on ELMs), it is likely that they will have to work together with symmetry breaking effects such as magnetic perturbations. Implications of magnetic perturbations for density control are still under investigation and will have to be addressed in both standard and advanced divertor configurations.

A characteristic impact of magnetic perturbations is the formation of helical lobes in the magnetic separatrix.[7,8] These helical lobes can intersect the divertor targets (or other wall elements) and can therefore directly impact particle and heat loads. We will address perturbations to the magnetic separatrix in Section III A. The perturbation field is resonant with the equilibrium field on a flux surface with a rational safety factor q, which leads to the formation of magnetic island chains.[30] These island chains can overlap and result in the formation of a chaotic (or sometimes referred to as "stochastic") layer from which field lines may escape all the way to the divertor targets. We will investigate the impact of advanced divertor configurations on this open boundary layer in Secs. III A and III B and discuss implications for plasma transport in Section IV. In the following, we will focus on configurations with an $n = 3$ perturbation field. Presently, we consider only the vacuum perturbation field as a start to provide an overview on possible configurations. Plasma response effects may be important,[31] and this overview is intended to identify a valuable configuration for a more detailed subsequent analysis.

A. Separatrix manifolds and their footprints

The application of a small non-axisymmetric magnetic perturbation results in the splitting of the magnetic separatrix into two distinct branches (see, e.g., Figure 1). This is a generic feature in non-linear systems[7] which is applicable within the framework of diverted tokamaks.[8] Let $\mathbf{L}_\mathbf{p}(l)$ be a magnetic field line through point $\mathbf{p}$ and l be the arc length long this field line, then the forward and backward branch of the separatrix associated with the X-point $\mathbf{X}$ are defined by

$$B^+ = \{\mathbf{p} | \lim_{l\to\infty} \mathbf{L}_\mathbf{p}(l) \to \mathbf{X}\} \tag{2}$$

and

$$B^- = \{\mathbf{p} | \lim_{l\to-\infty} \mathbf{L}_\mathbf{p}(l) \to \mathbf{X}\}, \tag{3}$$

respectively. These branches (often referred to as stable and unstable invariant manifolds associated with the X-point) determine where magnetic field lines may connect from the plasma interior to the divertor targets. Therefore, they can have a direct impact on divertor particle and heat loads.

A comparison of the separatrix manifolds resulting from a perturbation current of $I_c = 3$ kA is shown in Figure 4. A distinctive feature of the separatrix manifolds is the formation of helical lobes which can intersect the divertor targets (or other wall elements). These lobes can be characterized by their radial extension and poloidal width. The radial extension of the lobes is determined by the strength of the perturbation field, and it is the radial extension that defines the poloidal width of the perturbed magnetic footprint on the divertor target (see Figure 5). The Melnikov method (see, e.g., p. 202 in Ref. 7]) provides an efficient approach to estimate the divertor footprint.[32,33] The size $\mathcal{S} = \max_{\varphi_0} M(\varphi_0)$ can be approximated by the Melnikov-like function

$$M(\varphi_0) = \int_{-\infty}^{\infty} \frac{d\psi}{dl}\, dl. \tag{4}$$

The integral in (4) is taken along a field line on the unperturbed separatrix, where φ_0 is a reference toroidal angle for that field line. The integrand $\frac{d\psi}{dl}$ is calculated from the perturbation field and the separatrix geometry. $\mathcal{S}$ provides an estimate for the maximum radial extension of the separatrix lobes in a magnetic flux space. This needs to be combined with the magnetic flux expansion in the divertor to get the actual footprint size in real space. All cases have $\mathcal{S} \approx 0.024$ (except the neSF-case which is based on a different equilibrium), and thus

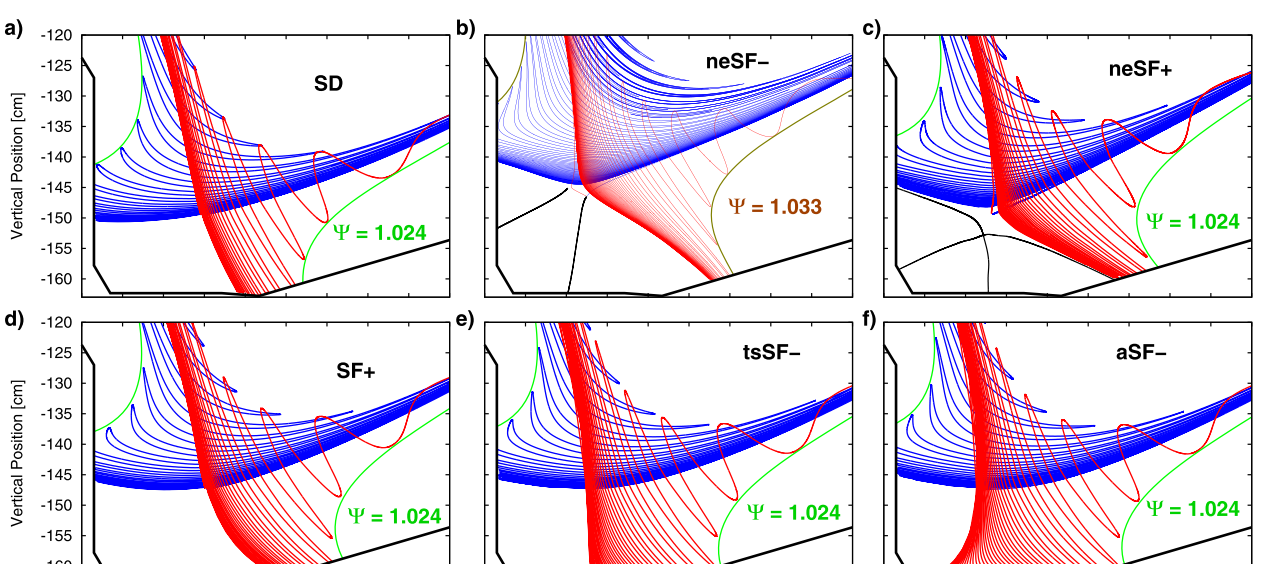

FIG. 4. Separatrix manifolds (blue: forward branch, red: backward branch) resulting from application of a 3 kA perturbation current to the base configurations from Figure 2. The $\psi = 1.024$ flux surface is marked in green for reference.

the lobes extend outward to $\psi \approx 1.024$. This can be seen in Figure 4 where the $\psi = 1.024$ surface is marked in green. As the flux expansion at the outer strike point is largest in the tsSF- and aSF-configurations, these have the largest separatrix footprint as well: $s_{\mathrm{tsSF-}} = 17.3\,\mathrm{cm}$ and $s_{\mathrm{aSF-}} \approx 25.6\,\mathrm{cm}$. Conversely, the flux expansion is smallest in the neSF configurations, resulting in a separatrix footprint of $s_{\mathrm{neSF-}} \approx 2.9\,\mathrm{cm}$ and $s_{\mathrm{neSF+}} \approx 5.7\,\mathrm{cm}$ which is smaller than the standard divertor configuration's $s_{\mathrm{SD}} \approx 8.4\,\mathrm{cm}$.

The spacing between the lobes is determined only by the equilibrium (for a given toroidal mode number n of the perturbation field) and not by the perturbation strength I_c. This is demonstrated in Figure 5 by increasing I_c from 1 kA to 4 kA. In the following, we will derive an approximation of the lobe width and the lobe spacing in the proximity of the X-point (as measured along the unperturbed separatrix). For that we consider the crossings between the perturbed and unperturbed separatrix as indicated in the sketch in Figure 1. Since B_{pol} is small when approaching the X-point, the change in R and Z along a field line is also small over one field period $2\pi/n$ and the perturbation is essentially a function of φ only. The net impact of the perturbation along a field line is cancelled out over one field period, and so the poloidal distance Δ_{pol} between two outward crossings (L_1 and L_2) or two inward

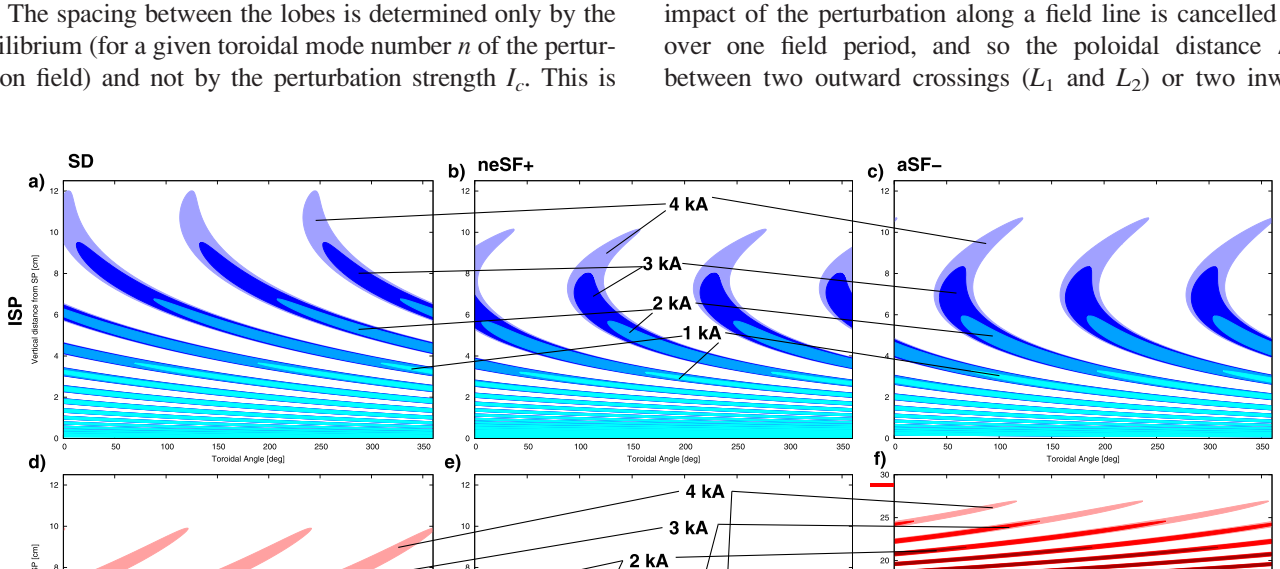

FIG. 5. Magnetic footprint of the perturbed separatrix at the inner strike point (ISP, upper row) and outer strike point (OSP, lower row): a comparison between the standard divertor (SD), near exact snowflake (neSF+), and X-divertor like (aSF-) configuration is shown while the perturbation strength is increased from 1 kA to 4 kA. Note the different scale in part (f).

crossings (M_1 and M_2) corresponds to the toroidal distance $\Delta_{\text{tor}} \approx 2\pi R / n$. The ratio of these distances can be approximated by the ratio of the local field components

$$\frac{\Delta_{\text{pol}}}{\Delta_{\text{tor}}} \approx \frac{B_{\text{pol}}}{B_{\text{tor}}}. \tag{5}$$

From that we find for the lobe density

$$\ell = \frac{1}{\Delta_{\text{pol}}} \approx \frac{n}{2\pi R} \frac{B_{\text{tor}}}{B_{\text{pol}}}, \tag{6}$$

i.e., the lobe density is determined by the toroidal symmetry of the perturbation field and by characteristics of the equilibrium configuration. A typical characteristic parameter for the plasma shape is the triangularity $\delta_X = \frac{R_0 - R_X}{a}$, where R_0 is the major radius of the magnetic axis, R_X is the major radius of the X-point, and a is the minor radius of the separatrix at the midplane. Another characteristic parameter is the aspect ratio $A = R_0/a$, and both can be used to relate the X-point position to the position of the magnetic axis

$$R_X = R_0 \left(1 - \frac{\delta_X}{A}\right). \tag{7}$$

Furthermore, let us assume $B_{\text{tor}} = B_0 R_0 / R$, then we find the asymptotic behavior of ℓ to be

$$\ell \approx \frac{n}{2\pi R_0} \frac{B_0}{B_{\text{pol}}} \left(1 - \frac{\delta_X}{A}\right)^{-2}, \tag{8}$$

which depends only on the scaling of the poloidal field (which is different for standard and snowflake divertors[22]). One implication of (8) is that triangularity plays a less important role in large aspect ratio devices such as DIII-D, but may be used in low aspect ratio devices (e.g., spherical tokamaks) to adjust the lobe density. A larger X-point triangularity results in a higher lobe density, which may facilitate heat flux spreading between lobes.

The lobe spacings Δ_{pol} for the different divertor configurations are shown in Figure 6. A clear linear scaling is found for the SD configuration, which is expected from the $B_{\text{pol}} \sim \rho$ scaling found in analytical models based on an expansion around the X-point. (ρ is the distance from the X-point). It can be seen that there are no significant differences between the "generalized snowflake" and the SD configurations, because these configurations are all based on the same equilibrium and the secondary X-point is far enough away. A $B_{\text{pol}} \sim \rho^2$ scaling is expected for a pure snowflake configuration,[22] and this is reflected in the lobe sizes of the near exact configurations. The difference between the neSF+ and neSF-configuration is related to the different equilibrium of the neSF-configuration, which is based on a plasma current of $I_p = 1$ MA rather than the 2 MA as in all other configurations.

B. Connection length and field line losses

The separatrix manifolds indicate the path along which field lines connect to the divertor targets, but they do not show from how deep inside the plasma these field lines connect from and over which distance this happens. SOL connections lengths are of the order $L_c \sim 50$ m, and field lines that connect within a similar distance from the plasma interior can be expected to have a significant impact on the edge plasma. The "openness" of the edge layer can be characterized by the field line loss fraction $\tau_L(\psi)$ from a former flux surface ψ: i.e., the fraction of field lines that connect from this radial location to the divertor targets with a given reference length L. Figure 7 demonstrates that the "openness" of the edge layer is not significantly affected by the divertor configuration. For all configurations, more than 50% of the field lines are lost within two SOL lengths from $\psi = 0.99$, but less than 10% are lost from inside $\psi = 0.96$ within that distance (see Figure 7). 10% of the field lines are still lost from $\psi = 0.83$ within $L = 1000$ m. While particle and heat diffusion may mitigate the impact of τ_L at such long distances, it should be kept in mind that the electron mean free path can become quite large due to the strong dependence on T_e. Fast parallel transport along open field lines provides a loss channel, and we find here (Figure 7) that there is no further degradation of field line confinement related to the

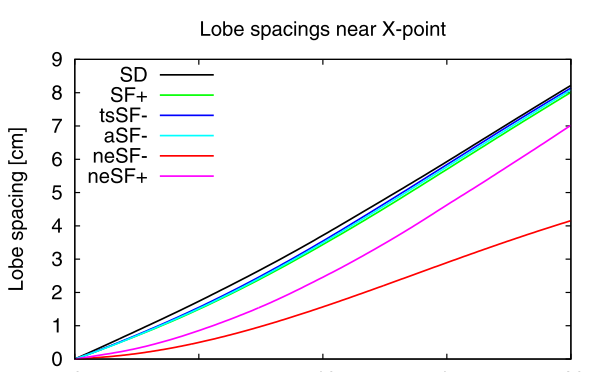

FIG. 6. Lobe spacings near the X-point, measured by the distance between two crossing points between the perturbed and unperturbed separatrix as sketched in Figure 1.

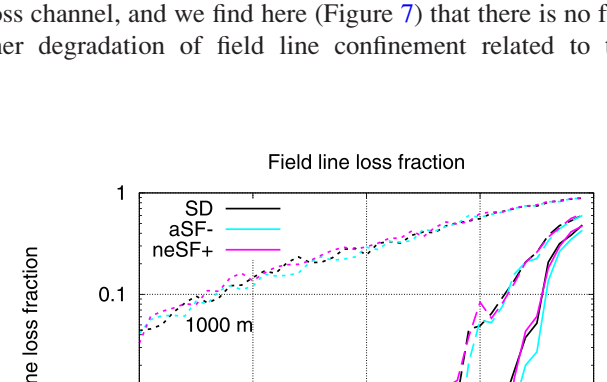

FIG. 7. Field line loss fraction $\tau_L(\psi)$ at a reference length of $L = 50$ m (solid), $L = 100$ m (dashed), and $L = 1000$ m (dotted): the three configurations shown are the standard divertor (SD), the near exact snowflake (neSF+), and the X-divertor like configuration (aSF-).

interaction between advanced divertor configurations and magnetic perturbations.

IV. IMPACT ON THE PLASMA EDGE

The non-axisymmetric nature of the perturbed magnetic configuration requires a three dimensional edge plasma model such as EMC3-EIRENE.[11,12] This code solves a set of steady-state Braginskii equations (EMC3) where anomalous cross-field transport is taken into account by free model parameters. Interactions with neutral gas are obtained from a kinetic transport model (EIRENE). EMC3-EIRENE is based on a reversible field line mapping technique,[34] and combined with a block-structured decomposition of the edge plasma domain[13] which allows a detailed analysis of RMP related features in poloidal divertor tokamaks.[35,36] It has recently been implemented at NSTX[15] for standard divertor configurations with RMPs, and at TCV for axisymmetric snowflake divertors configurations.[37]

In the following, we use EMC3-EIRENE to investigate the resulting impact of the interaction between magnetic perturbations and advanced divertor configurations on the edge plasma. All simulations are based on a fixed core refuelling rate of $\Gamma_{\mathrm{ISB}} \approx 3.1 \times 10^{20}\,\mathrm{s}^{-1}$ (50 A) and a fixed recycling coefficient of $c_{\mathrm{rec}} = 0.99$. The edge power input is set to $P_{\mathrm{in}} = 2\,\mathrm{MW}$, and diffusion coefficients for anomalous cross-field transport are set to $D_{\perp} = 0.3\,\mathrm{m}^2\,\mathrm{s}^{-1}$ and $\chi_e = \chi_i = 2\,\mathrm{m}^2\,\mathrm{s}^{-1}$. Impurity production and transport are neglected at this point. The inner simulation boundary is located at the last closed magnetic flux surface at $\psi \approx 0.6$ in the perturbed configurations and set at $\psi = 0.99$ in the unperturbed reference configurations.

A comparison between the perturbed and unperturbed edge plasma density is shown in Figure 8 for a few selected configurations (compare upper row vs. lower row). It can be seen that all cases operate in a "high recycling" regime where the downstream density at the strike points is larger than the upstream density. The remaining configurations from Figure 2 show the same behavior. The plasma density in the RMP cases follows the lobe structure of the perturbed separatrix manifold which connects to the outer strike point. In contrast, such a pattern cannot be seen at the inner strike point at the given level for anomalous cross-field transport. This is distinct from findings at large aspect ratio tokamaks such as DIII-D,[38] but consistent with initial simulations for NSTX (see Figure 4(c) in Ref. 15). Since spatial scales (e.g., toroidal separation between lobes) are much smaller on the high field side of low aspect ratio devices, diffusion may lead to a wash-out at the inner strike point. Indeed, particle and heat loads patterns at the inner strike point are essentially axisymmetric and do not follow the lobe pattern of the magnetic footprint. This is demonstrated in Figure 9(a) for the SF+ configuration, and it is found in the other configurations as well. Heat flux profiles at a fixed toroidal location are shown in Figure 9(b), and it is found that the heat flux in the perturbed configuration (blue) matches the heat flux in unperturbed configuration (red). At the outer strike point, on the other hand, formation of a non-axisymmetric striation pattern is found, which is visualized in Figures 9(c) and 9(d) for the SF+ configuration. Heat load peaks occur at the locations where field lines connect to the interior, which is indicated by the gray line. In the following, we will focus on the outer strike point (OSP).

A. Unperturbed heat loads

Profiles of the heat loads at $\varphi = 0°$ are shown in Figure 10(a) for a direct comparison between the different divertor configurations. The unperturbed standard divertor configuration (black) exhibits a peak heat load of about $2.3\,\mathrm{MW\,m^{-2}}$ which is located—as expected—just outside the separatrix strike point. The heat loads are significantly mitigated in the generalized SF-configurations, which is consistent with a large flux expansion (compare Figure 3(a)). These are the configurations that can be regarded as X-divertor at the OSP. The tsSF-configuration (blue) has the secondary X-point just outside the primary separatrix strike point, which is where the largest flux expansion occurs. Consequently, heat loads at the separatrix strike point are very small ($0.6 - 0.7\,\mathrm{MW\,m^{-2}}$), and the peak heat load of $1.35\,\mathrm{MW\,m^{-2}}$ occurs at a distance of 15 cm away from the separatrix strike point where the flux expansion has become significantly smaller. The secondary X-point in the aSF-configuration (cyan) is located further

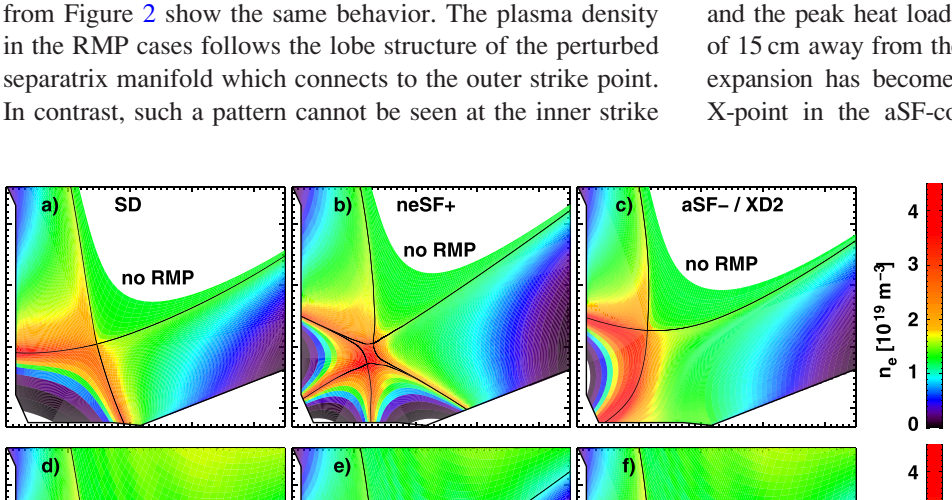

FIG. 8. Comparison of the edge plasma density with and without magnetic perturbations: (a) and (d) standard divertor configuration, (b) and (e) near exact snowflake configuration, and (c) and (f) asymmetric snowflake minus/X-divertor configuration. The position of the unperturbed separatrix is marked in black for reference.

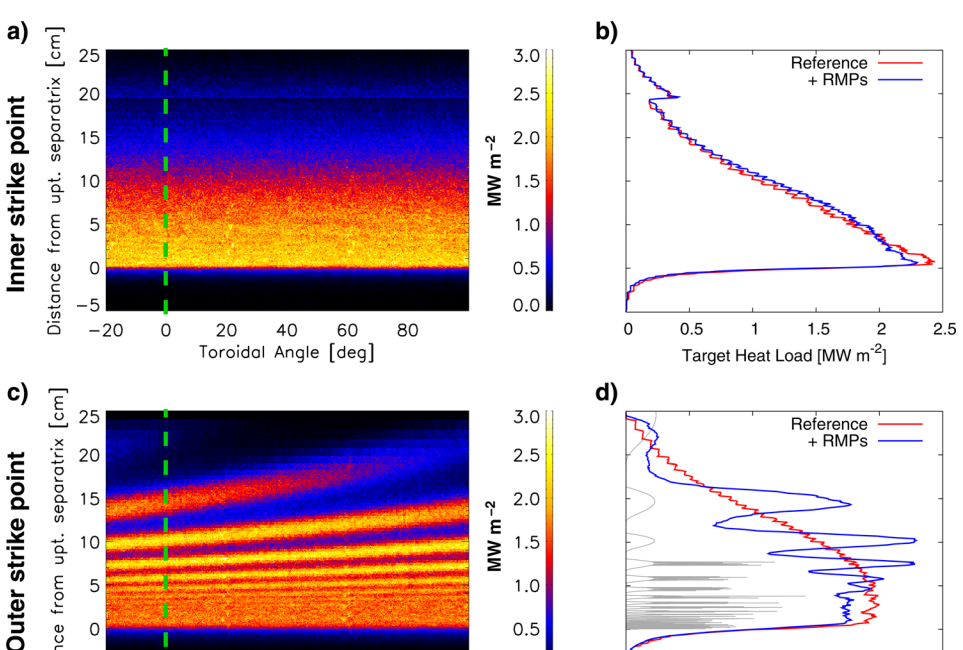

FIG. 9. Divertor heat loads at the inner and outer strike point for the SF+ case, the 1D profiles are extracted at $\varphi = 0\,^{\circ}$.

outside, which results in a maximal flux expansion and minimal heat load about 10 cm away from the separatrix strike point: the main heat flux peak of 1 MW m^{-2} at the separatrix is reduced to 0.22 MW m^{-2} by the increase in flux expansion, after which flux expansion decreases again faster than the heat load dissipates, and thus resulting in a secondary (albeit axisymmetric) peak about 25 cm away from the separatrix strike point. The near exact snowflake configurations (red, magenta), on the other hand, feature an increase of the peak heat load up to 7 MW m^{-2} in the neSF-configuration. This is consistent with a smaller flux expansion at the divertor target in those configurations than in the SD configuration. Almost no heat is deposited at secondary separatrix strike points.

B. Perturbed heat loads

The application of RMPs, as shown in Figure 10(b), results in non-axisymmetric striation patterns with secondary heat load peaks. Peaks can be a few cm apart, but generally occur only where the flux expansion is locally not too large. Huge flux expansion occurs in the tsSF- and aSF-cases next to the separatrix strike point: i.e., $d_{\mathrm{mid}} = 2$ mm expands to

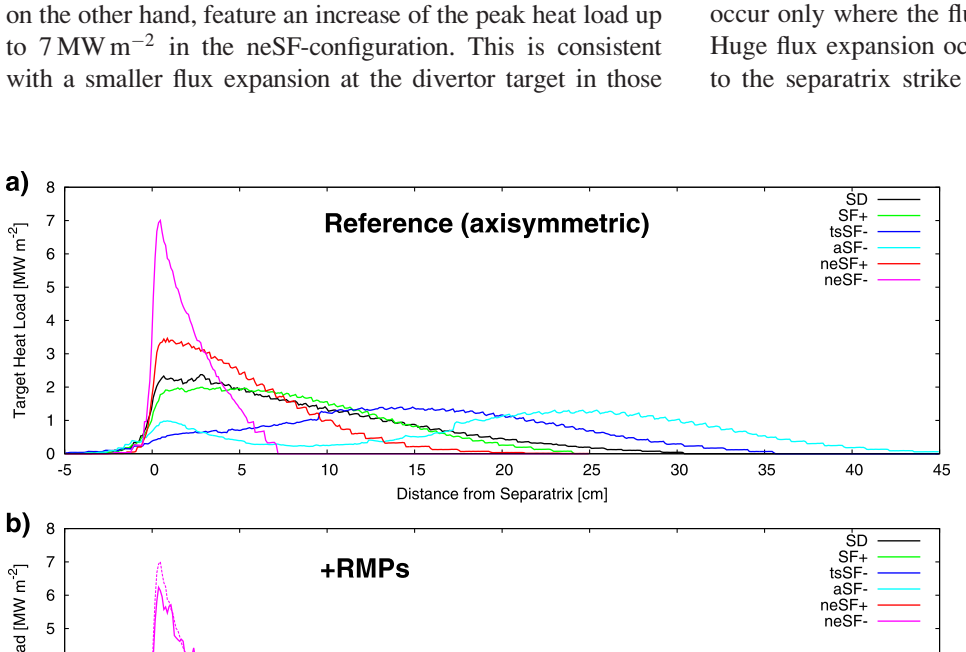

FIG. 10. Heat loads at the outer strike point: (a) the axisymmetric reference cases and (b) the RMP cases where profiles from (a) have been superimposed as dashed lines for comparison.

$d_{target} = 12\,cm$ ($F_{tsSF-} = 60$) and $20\,cm$ ($F_{aSF-} = 100$), respectively. Further outside, however, flux expansion drops to more moderate values. Heat loads in the aSF-configuration (cyan) with and without RMPs are nearly identical up to 22 cm away from the separatrix strike point. The magnetic footprint does have a distinct striation pattern in this region, but the huge upstream to downstream flux expansion means that a small amount of diffusion upstream suffices to smear out particle and heat loads on the divertor target. Only the outermost part of the magnetic footprint is reflected in the heat load footprint since the flux expansion drops to more moderate values here. These peaks can still be significant: e.g., $q_t = 2\,MW$ at $d_{target} \approx 20\,cm$ in the tsSF-case (blue) with RMPs while $q_t = 1.2\,MW$ in the corresponding unperturbed case. For weaker magnetic perturbations (i.e., so that the lobes do not extend beyond the region of huge flux expansion), or with careful adjustment of the local flux expansion, it might be possible to avoid the formation of secondary, non-axisymmetric heat flux peaks. Nevertheless, a finite level of "unperturbed" heat flux remains at these locations.

The near exact snowflake configurations have secondary heat flux peaks as well when RMPs are applied, although the footprint is much smaller due to the relatively small flux expansion compared to the standard divertor case. The main peak is reduced by about 10%, which is still by a factor of 3 larger than in the reference case. There is no redistribution of heat flux from the primary to the secondary strike points, essentially because there is no interaction between the primary and secondary separatrix manifolds.

V. CONCLUSIONS

The flexible setup at NSTX-U allows for a variety of divertor configurations, including near exact snowflake configurations as well as SF plus and minus variations. However, the snowflake classifications are based on the magnetic topology alone and do not take into account the relative position of the divertor plates. In fact, we find that implementations of the snowflake minus configuration at NSTX-U can have the secondary X-point behind the wall, and thus act like an X-divertor at the outer strike point. While one of the originally intended features of the snowflake configuration is an increased flux expansion introduced around the X-point, we find that near exact snowflake implementations at NSTX-U can have a reduced flux expansion at the target with respect to the standard divertor configuration. We find that these configurations exhibit heat flux peaking by a factor of up to 3, while almost no heat load is found at the secondary strike points. The X-divertor like configurations have more flux expansion on the divertor target than the standard divertor configuration, and the heat loads are modified accordingly. Peak heat loads are reduced by $40\% - 45\,\%$, and their location is shifted $15 - 25\,cm$ away from the separatrix strike point depending on the local flux expansion. Magnetic perturbations introduce non-axisymmetric heat loads only at the outer strike point since the toroidal separation between lobes is much smaller on the high field side in low aspect ratio devices. Large flux expansion on the target allows for expansion of the magnetic footprint. While the magnifying impact of flux expansion on the lobe structure may invite to use these configurations as benchmark for plasma response effects, conclusions from the absence of corresponding peaks in experimentally observed plasma footprints may be misleading. This is because a small amount of diffusion upstream suffices to smear out particle and heat loads on the divertor target, so that only the outermost part of the footprint—where flux expansion drops to a moderate levels—is reflected in the plasma. For weaker magnetic perturbations, or with careful adjustment of the local flux expansion, it might be possible to avoid the formation of secondary, non-axisymmetric heat flux peaks.

ACKNOWLEDGMENTS

This work was supported in part by the U.S. Department of Energy under DE-SC0012315 and DE-FC02-04ER54698, and by Start-Up Funds of the University of Wisconsin—Madison. The digital data for this paper can be found in http://arks.princeton.edu/ark:/88435/dsp018p58pg29j.

[1]T. E. Evans, R. A. Moyer, K. H. Burrell, M. E. Fenstermacher, I. Joseph, A. W. Leonard, T. H. Osborne, G. D. Porter, M. J. Schaffer, P. B. Snyder, P. R. Thomas, J. G. Watkins, and W. P. West, "Edge stability and transport control with resonant magnetic perturbations in collisionless tokamak plasmas," Nat. Phys. **2**, 419–423 (2006).

[2]Y. Liang, H. R. Koslowski, P. R. Thomas, E. Nardon, B. Alper, P. Andrew, Y. Andrew, G. Arnoux, Y. Baranov, M. Becoulet, M. Beurskens, T. Biewer, M. Bigi, K. Crombe, E. De La Luna, P. de Vries, W. Fundamenski, S. Gerasimov, C. Giroud, M. P. Gryaznevich, N. Hawkes, S. Hotchin, D. Howell, S. Jachmich, V. Kiptily, L. Moreira, V. Parail, S. D. Pinches, E. Rachlew, and O. Zimmermann, "Active Control of Type-I Edge-Localized Modes with n = 1 Perturbation Fields in the JET Tokamak," Phys. Rev. Lett. **98**, 265004 (2007).

[3]W. Suttrop, T. Eich, J. C. Fuchs, S. Günter, A. Janzer, A. Herrmann, A. Kallenbach, P. T. Lang, T. Lunt, M. Maraschek, R. M. McDermott, A. Mlynek, T. Pütterich, M. Rott, T. Vierle, E. Wolfrum, Q. Yu, I. Zammuto, H. Zohm, and ASDEX Upgrade Team, "first observation of edge localized modes mitigation with resonant and nonresonant magnetic perturbations in ASDEX upgrade," Phys. Rev. Lett. **106**, 225004 (2011).

[4]A. Loarte, G. Huijsmans, S. Futatani, L. R. Baylor, T. E. Evans, D. M. Orlov, O. Schmitz, M. Becoulet, P. Cahyna, Y. Gribov, A. Kavin, A. Sashala Naik, D. J. Campbell, T. Casper, E. Daly, H. Frerichs, A. Kischner, R. Laengner, S. Lisgo, R. A. Pitts, G. Saibene, and A. Wingen, "Progress on the application of ELM control schemes to ITER scenarios from the non-active phase to DT operation," Nucl. Fusion **54**, 033007 (2014).

[5]T. E. Evans, "Resonant magnetic perturbations of edge-plasmas in toroidal confinement devices," Plasma Phys. Controlled Fusion **57**, 123001 (2015).

[6]J. M. Canik, R. Maingi, T. E. Evans, R. E. Bell, S. P. Gerhardt, B. P. LeBlanc, J. Manickam, J. E. Menard, T. H. Osborne, J.-K. Park, S. F. Paul, P. B. Snyder, S. A. Sabbagh, H. W. Kugel, E. A. Unterberg, and the NSTX Team, "On demand triggering of edge localized instabilities using external nonaxisymmetric magnetic perturbations in toroidal plasmas," Phys. Rev. Lett. **104**, 045001 (2010).

[7]J. Guckenheimer and P. Holmes, *Nonlinear Oscillations, Dynamical Systems, and Bifurcations of Vector Fields* (Applied Mathematical Science, 1983).

[8]T. E. Evans, R. K. W. Roeder, J. A. Carter, and B. I. Rapoport, "Homoclinic tangles, bifurcations and edge stochasticity in diverted tokamaks," Contrib. Plasma Phys. **44**, 235–240 (2004).

[9]T. E. Evans, R. K. W. Roeder, J. A. Carter, B. I. Rapoport, M. E. Fenstermacher, and C. J. Lasnier, "Experimental signatures of homoclinic tangles in poloidally diverted tokamaks," J. Phys. Conf. Ser. **7**, 174 (2005).

[10]J-W. Ahn, R. Maingi, J. M. Canik, A. G. McLean, J. D. Lore, J.-K. Park, V. A. Soukhanovskii, T. K. Gray, and A. L. Roquemore, "Effect of nonaxisymmetric magnetic perturbations on divertor heat and particle flux profiles in National Spherical Torus Experiment," Phys. Plasmas **18**, 056108 (2011).

[11]Y. Feng, F. Sardei, J. Kisslinger, P. Grigull, K. McCormick, and D. Reiter, "3D edge modeling and island divertor physics," Contrib. Plasma Phys. **44**(1–3), 57–69 (2004).
[12]Y. Feng, H. Frerichs, M. Kobayashi, A. Bader, F. Effenberg, D. Harting, H. Hoelbe, J. Huang, G. Kawamura, J. D. Lore, T. Lunt, D. Reiter, O. Schmitz, and D. Sharma, "Recent improvements in the EMC3-eirene code," Contrib. Plasma Phys. **54**(4–6), 426–431 (2014).
[13]H. Frerichs, D. Reiter, Y. Feng, and D. Harting, "Block-structured grids in Lagrangian 3D edge plasma transport simulations," Comput. Phys. Commun. **181**, 61–70 (2010).
[14]T. Lunt, Y. Feng, M. Bernet, A. Herrmann, P. de Marne, R. McDermott, H. W. Müller, S. Potzel, T. Pütterich, S. Rathgeber, W. Suttrop, E. Viezzer, E. Wolfrum, M. Willensdorfer, and the ASDEX Upgrade team, "First EMC3-Eirene simulations of the edge magnetic perturbations at ASDEX upgrade compared with the experiment," Nucl. Fusion **52**, 054013 (2012).
[15]J. D. Lore, J. M. Canik, Y. Feng, J.-W. Ahn, R. Maingi, and V. Soukhanovskii, "Implementation of the 3D edge plasma code EMC3-EIRENE on NSTX," Nucl. Fusion **52**, 054012 (2012).
[16]O. Schmitz, M. Becoulet, P. Cahyna, T. E. Evans, Y. Feng, H. Frerichs, A. Loarte, R. A. Pitts, D. Reiser, M. E. Fenstermacher, D. Harting, A. Kirschner, A. Kukushkin, T. Lunt, G. Saibene, D. Reiter, U. Samm, and S. Wiesen, "Three-dimensional modeling of plasma edge transport and divertor fluxes during application of resonant magnetic perturbations on ITER," Nucl. Fusion **56**, 066008 (2016).
[17]W. Engelhardt and W. Feneberg, "Influence of an ergodic magnetic limiter on the impurity content in a tokamak," J. Nucl. Mater. **76–77**, 518–520 (1978).
[18]W. Feneberg and G. H. Wolf, "A helical magnetic limiter for boundary layer control in large tokamaks," Nucl. Fusion **21**, 669–675 (1981).
[19]D. D. Ryutov, "Geometrical properties of as 'snowflake' divertor," Phys. Plasmas **14**, 064502 (2007).
[20]M. Kotschenreuther, P. M. Valanju, S. M. Mahajan, and J. C. Wiley, "On heat load, novel divertors, and fusion reactors," Phys. Plasmas **14**, 072502 (2007).
[21]P. M. Valanju, M. Kotschenreuther, S. M. Mahajan, and J. Canik, "Super-X divertors and high power density fusion devices," Phys. Plasmas **16**, 056110 (2009).
[22]D. D. Ryutov, R. H. Cohen, T. D. Rognlien, and M. V. Umansky, "The magnetic field structure of a snowflake divertor," Phys. Plasmas **15**, 092501 (2008).
[23]D. D. Ryutov, M. A. Makowski, and M. V. Umansky, "Local properties of the magnetic field in a snowflake divertor," Plasma Phys. Controlled Fusion **52**, 105001 (2010).
[24]M. Kotschenreuther, P. Valanju, B. Covele, and S. Mahajan, "Magnetic geometry and physics of advanced divertors: The X-divertor and the snowflake," Phys. Plasmas **20**, 102507 (2013).
[25]D. D. Ryutov, R. H. Cohen, T. D. Rognlien, V. A. Soukhanovskii, and M. V. Umansky, "Comment on "Magnetic geometry and physics of advanced divertors: The X-divertor and the snowflake," Phys. Plasmas **21**, 054701 (2014).
[26]M. Kotschenreuther, P. Valanju, B. Covele, and S. Mahajan, "Response to 'Comment on Magnetic geometry and physics of advanced divertors: The X-divertor and the snowflake,'" Phys. Plasmas **21**, 054702 (2014).
[27]J. E. Menard, S. Gerhardt, M. Bell, J. Bialek, A. Brooks, J. Canik, J. Chrzanowski, M. Denault, L. Dudek, D. A. Gates, N. Gorelenkov, W. Guttenfelder, R. Hatcher, J. Hosea, R. Kaita, S. Kaye, C. Kessel, E. Kolemen, H. Kugel, R. Maingi, M. Mardenfeld, D. Mueller, B. Nelson, C. Neumeyer, M. Ono, E. Perry, R. Ramakrishnan, R. Raman, Y. Ren, S. Sabbagh, M. Smith, V. Soukhanovskii, T. Stevenson, R. Strykowsky, D. Stutman, G. Taylor, P. Titus, K. Tresemer, K. Tritz, M. Viola, M. Williams, R. Woolley, H. Yuh, H. Zhang, Y. Zhai, A. Zolfaghari, and the NSTX Team, "Overview of the physics and engineering design of NSTX upgrade," Nucl. Fusion **52**, 083015 (2012).
[28]T. E. Evans, D. M. Orlov, A. Wingen, W. Wu, A. Loarte, T. A. Casper, O. Schmitz, G. Saibene, M. J. Schaffer, and E. Daly, "3D vacuum magnetic field modelling of the ITER ELM control coil during standard operating scenarios," Nucl. Fusion **53**, 093029 (2013).
[29]O. Schmitz, T. E. Evans, M. E. Fenstermacher, M. J. Lanctot, C. L. Lasnier, S. Mordijck, R. A. Moyer, H. Reimerdes, and the DIII-D Team, "Formation of a three-dimensional plasma boundary after decay of the plasma response to resonant magnetic perturbation fields," Nucl. Fusion **54**(1), 012001 (2014).
[30]O. Schmitz, T. E. Evans, M. E. Fenstermacher, H. Frerichs, M. W. Jakubowski, M. J. Schaffer, A. Wingen, W. P. West, N. H. Brooks, K. H. Burrell, J. S. deGrassie, Y. Feng, K. H. Finken, P. Gohil, M. Groth, I. Joseph, C. J. Lasnier, M. Lehnen, A. W. Leonard, S. Mordijck, R. A. Moyer, A. Nicolai, T. H. Osborne, D. Reiter, U. Samm, K. H. Spatschek, H. Stoschus, B. Unterberg, E. A. Unterberg, J. G. Watkins, R. Wolf, and the DIII-D and TEXTOR Teams, "Aspects of three dimensional transport for ELM control experiments in ITER-similar shape plasmas at low collisionality in DIII-D," Plasma Phys. Controlled Fusion **50**, 124029 (2008).
[31]J.-K. Park, A. H. Boozer, J. E. Menard, A. M. Garofalo, M. J. Schaffer, R. J. Hawryluk, S. M. Kaye, S. P. Gerhardt, S. A. Sabbagh, and NSTX Team, "Importance of plasma response to nonaxisymmetric perturbations in tokamaks," Phys. Plasmas **16**, 056115 (2009).
[32]P. Cahyna and E. Nardon, "Resonant magnetic perturbations and divertor footprints in poloidally diverted tokamaks," e-print arXiv:1005.3663 [physics.plasm-ph].
[33]P. Cahyna, M. Peterka, E. Nardon, H. Frerichs, and R. Panek, "Method for comparison of tokamak divertor strike point data with magnetic perturbation models," Nucl. Fusion **54**, 064002 (2014).
[34]Y. Feng, F. Sardei, and J. Kisslinger, "A simple highly accurate field-line mapping technique for three-dimensional Monte Carlo modeling of plasma edge transport," Phys. Plasmas **12**, 052505 (2005).
[35]H. Frerichs, D. Reiter, O. Schmitz, T. E. Evans, and Y. Feng, "Three-dimensional edge transport simulations for DIII-D plasmas with resonant magnetic perturbations," Nucl. Fusion **50**, 034004 (2010).
[36]H. Frerichs and D. Reiter, "Stability and control of iterated non-linear transport solvers for fusion edge plasmas," Comput. Phys. Commun. **188**, 82 (2015).
[37]T. Lunt, G. P. Canal, Y. Feng, H. Reimerdes, B. P. Duval, B. Labit, W. A. J. Vijvers, D. Coster, K. Lackner, and M. Wischmeier, "First EMC3-Eirene simulations of the TCV snowflake divertor," Plasma Fusion Res. **56**, 035009 (2014).
[38]H. Frerichs, O. Schmitz, T. Evans, Y. Feng, and D. Reiter, "The pattern of parallel edge plasma flows due to pressure gradients, recycling, and resonant magnetic perturbations in DIII-D," Phys. Plasmas **22**, 072508 (2015).